Supporting Information

Endo et al. 10.1073/pnas.1505683112

SI Materials and Methods

Mice. Wild-type C57BL/6NtacfBR mice were purchased from Charles River Laboratories or from Taconic Farms. As described previously (1), *Stra8*-mutant mice (2) were crossed to C57BL/6 mice for at least 15 generations. In these back-crossed mice, >99.99% of the genome is expected to be of C57BL/6 origin; all Y chromosomes and mitochondria are of C57BL/6 origin. *Stra8*-deficient males were generated by mating heterozygotes. *Stra8* genotypes were assayed by PCR as described previously (2). *Dmc1*-deficient mice (3) (strain name B6.Cg-Dmc1^{tm1Jcs}/JcsJ) were purchased from the Jackson Laboratory. The *Dmc1*-deficient mice were back-crossed to C57BL/6J mice for at least 10 generations. *Dmc1*-deficient males were generated by mating heterozygotes. *Dmc1* genotypes were assayed by PCR, using the protocol provided by the Jackson Laboratory.

mRNA-Seq and Microarray Data Analysis. For mRNA-Seq data, reads were aligned to the mouse genome (mm9, NCBI Build 37) using TopHat (4). Unique reads in each gene were counted using htseq-count (5). For genome-wide differential expression analysis, fold changes and *P* values were calculated using edgeR, using tagwise dispersions and normalizing for library complexity (6). For genome-wide clustering analysis, FPKM (fragments per kilobase per million fragments mapped) values were calculated using Cufflinks (7) or downloaded directly (8, supplemental dataset S1); then, complete linkage hierarchical clustering, based on Spearman correlations of the FPKM values, was performed using custom R scripts. For marker gene analysis, read counts were normalized to the 75th percentile as described in Bullard et al. (9), and *P* values were calculated using Welch's *t* test. For microarray data, the microarray CEL files were normalized with the GCRMA package from Bioconductor. Probe set names were mapped to gene names using Bioconductor's mouse4302.db package and DAVID (10, 11). When multiple probe sets mapped to the same gene, absent probe sets were filtered out and then the median was used (12). Replicate arrays were averaged using limma (13). To compare the datasets (Fig. 2*C* and Fig. S2*E*), the genes present in both datasets were analyzed. Each gene was categorized based on the cell type of maximum expression. If a gene had equally high expression in two or more germ-cell types, it was not counted toward any cell type.

Identification of the Stages of the Seminiferous Cycle. Seminiferous stages were determined using PAS and hematoxylin-stained cross-sections, according to morphological criteria (14, 15). In brief, 12 stages were determined primarily based on the first 12 steps of spermatid development. When the patterns of germ-cell associations were changed after RA injection, the stages were identified according to spermatid development. The stages in immunohistochemically stained sections were determined using adjacent serial sections stained with PAS and hematoxylin (Fig. S1*B*).

Immunostaining on Testis Sections. Testes were fixed overnight in Bouin's solution at room temperature (for colorimetric detection, and for fluorescent detection of LIN28A) or in 4% paraformaldehyde at 4 °C (for all other fluorescent detection). Primary and secondary antibodies are listed in Table S3, along with incubation and blocking conditions. ImmPRESS peroxidase reagents are from Vector Laboratories and PowerVision Poly-HRP conjugated secondary antibodies are from Leica Biosystems. Unless otherwise noted, all other secondary antibodies are donkey antibodies from Jackson ImmunoResearch Laboratories. For LIN28A-strained slides with fluorescent detection, after incubation with the secondary antibody, slides were washed with PBS and incubated for 60 min at room temperature with donkey anti-streptavidin antibody (1:200 dilution) conjugated to FITC (Jackson ImmunoResearch Laboratories). For colorimetric detection, slides were developed using a DAB substrate kit (Vector Laboratories), counterstained with Mayer's hematoxylin, dehydrated, and mounted with Permount (Fisher Scientific). For fluorescent detection, slides were mounted with Vectashield mounting media with DAPI (Vector Laboratories).

Immunostaining on Intact Testis Tubules. The combinations of primary and secondary antibodies are as follows. Anti-STRA8 (1:500 dilution; ab49405, Abcam) with donkey anti-rabbit antibody conjugated to FITC (1:200 dilution; Jackson ImmunoResearch Laboratories); anti-PLZF (1:100 dilution; OP128, Calbiochem) with donkey anti-mouse antibody conjugated to Rhodamine Red X (1:200 dilution; Jackson ImmunoResearch Laboratories); and anti-GFRα1 (1:100 dilution; AF560, R&D Systems) with donkey anti-goat antibody conjugated to Dylight 649 (1:1,000 dilution; Rockland Immunochemicals).

SI Results and Discussion

Expression Patterns of Aged *Stra8*-Deficient Testes Are Similar to Those of Type A Spermatogonia. To verify that the aged *Stra8*-deficient testes were composed of type A spermatogonia, we computed genome-wide expression correlations between our mRNA-Seq data and three publically available germ-cell datasets (Fig. S2*B*). First, we compared with microarray data from sorted type A and B spermatogonia, pachytene spermatocytes, and round spermatids (16) (also used in Fig. 2*C*). Second, we compared with mRNA-Seq data from primary cultures of THY1-positive (undifferentiated type A) spermatogonia, looking at both Id4-GFP–positive (stem-like) and Id4-GFP–negative (not stem-like) fractions (8) (SRA accession no. SRP042067). Finally, we compared with mRNA-Seq data from sorted Oct4-GFP-positive (type A) spermatogonia, looking at both KIT-negative (undifferentiated) and KIT-positive (differentiating) fractions (SRA accession no. DRP002386). The expression patterns of *Stra8*-deficient testis were highly correlated with expression patterns of the other type A spermatogonial samples (correlations ranging from 0.75 to 0.91). When we clustered samples from the four datasets, the *Stra8*-deficient testis clustered in the middle of other type A spermatogonial samples. These results suggest that the expression patterns of *Stra8*-deficient testis are typical of type A spermatogonia.

Aged *Stra8*-Deficient Testes Up-Regulate Markers of Undifferentiated Spermatogonia. Given that young *Stra8*-deficient testes progressively accumulate undifferentiated spermatogonia, we predicted that aged *Stra8*-deficient testes would consist in large part of undifferentiated spermatogonia. We thus assessed the expression of marker genes in these aged testes. Our whole-testis mRNA-Seq data confirmed that genes expressed in undifferentiated spermatogonia were up-regulated in aged *Stra8*-deficient testes (relative to wild-type testes) (Fig. S2*C*). However, we also observed some up-regulation of genes expressed in early differentiating spermatogonia (*Kit* and *Ccnd2*). We next immunostained for KIT and for three markers of undifferentiated spermatogonia: LIN28A (17), PLZF (also known as ZBTB16) (18, 19), and GFRα1 (8, 20) (Fig. S2*D*). All three undifferentiated markers were highly expressed in aged *Stra8*-deficient testes, with little cell-to-cell

heterogeneity, whereas expression of KIT was patchy. This mixed expression pattern could be a result of ongoing partial differentiation within the aged *Stra8*-deficient testes, or could be a secondary effect of perturbed soma–germ interaction in these massively enlarged testes. To confirm that the *Stra8*-deficient spermatogonial accumulations were more similar to undifferentiated than to differentiating spermatogonia, we performed genome-wide analyses. As expected, in our genome-wide correlation analysis (Fig. S2*B*), *Stra8*-deficient testis was more closely correlated with KIT-negative (undifferentiated) spermatogonia than with KIT-positive (early differentiating) spermatogonia. When we looked specifically at the 100 genes most significantly up-regulated in *Stra8*-deficient vs. wild-type testes (Fig. S2*E* and Table S1), we found that 70% were more highly expressed in KIT-negative than in KIT-positive spermatogonia ($P = 0.002$, compared with a control of all analyzable genes in the mRNA-Seq dataset, Fisher's exact test). Similarly, 70% were more highly expressed in Id4-GFP–positive than in Id4-GFP–negative spermatogonia ($P < 0.001$) (8). These strong similarities in expression between undifferentiated spermatogonia and the aged *Stra8*-deficient testes are consistent with an accumulation of undifferentiated spermatogonia in aged *Stra8*-deficient mice.

The Precocious Leptotene Spermatocytes Could Progress Normally Through Meiosis. In the unperturbed testis, after meiotic initiation, germ cells develop into zygotene spermatocytes and ultimately undergo meiotic divisions, after 4 and 12.25 d, respectively (Fig. S6*A*). We expected to see transient increases in these cell types after RA injection. Indeed, at 4 d after RA injections, zygotene spermatocytes were present in a broader range of stages (IX–XII) than in control testes (X–XII) (Fig. S6 *B* and *C*). Similarly, at 12.25 d after RA injection, meiotically dividing spermatocytes were present in an increased fraction of testis tubules, throughout stages X–XII, compared with XII in control testes (Fig. S6 *D* and *E*).

1. Anderson EL, et al. (2008) *Stra8* and its inducer, retinoic acid, regulate meiotic initiation in both spermatogenesis and oogenesis in mice. *Proc Natl Acad Sci USA* 105(39): 14976–14980.
2. Baltus AE, et al. (2006) In germ cells of mouse embryonic ovaries, the decision to enter meiosis precedes premeiotic DNA replication. *Nat Genet* 38(12):1430–1434.
3. Pittman DL, et al. (1998) Meiotic prophase arrest with failure of chromosome synapsis in mice deficient for *Dmc1*, a germline-specific RecA homolog. *Mol Cell* 1(5):697–705.
4. Trapnell C, Pachter L, Salzberg SL (2009) TopHat: Discovering splice junctions with RNA-Seq. *Bioinformatics* 25(9):1105–1111.
5. Anders S, Pyl PT, Huber W (2015) HTSeq—a Python framework to work with high-throughput sequencing data. *Bioinformatics* 31(2):166–169.
6. Robinson MD, McCarthy DJ, Smyth GK (2010) edgeR: A Bioconductor package for differential expression analysis of digital gene expression data. *Bioinformatics* 26(1): 139–140.
7. Trapnell C, et al. (2010) Transcript assembly and quantification by RNA-Seq reveals unannotated transcripts and isoform switching during cell differentiation. *Nat Biotechnol* 28(5):511–515.
8. Chan F, et al. (2014) Functional and molecular features of the Id4+ germline stem cell population in mouse testes. *Genes Dev* 28(12):1351–1362.
9. Bullard JH, Purdom E, Hansen KD, Dudoit S (2010) Evaluation of statistical methods for normalization and differential expression in mRNA-Seq experiments. *BMC Bioinformatics* 11:94.
10. Huang W, Sherman BT, Lempicki RA (2009) Bioinformatics enrichment tools: Paths toward the comprehensive functional analysis of large gene lists. *Nucleic Acids Res* 37(1):1–13.
11. Huang W, Sherman BT, Lempicki RA (2009) Systematic and integrative analysis of large gene lists using DAVID bioinformatics resources. *Nat Protoc* 4(1):44–57.
12. Cui X, Loraine AE (2009) Consistency analysis of redundant probe sets on affymetrix three-prime expression arrays and applications to differential mRNA processing. *PLoS ONE* 4(1):e4229.
13. Smyth GK (2005) limma: Linear models for microarray data. *Bioinformatics and Computational Biology Solutions Using R and Bioconductor*, eds Gentleman R, Carey VJ, Huber W, Irizarry RA, Dudoit S (Springer, New York), pp 397–420.
14. Oakberg EF (1956) A description of spermiogenesis in the mouse and its use in analysis of the cycle of the seminiferous epithelium and germ cell renewal. *Am J Anat* 99(3): 391–413.
15. Russell LD, Ettlin RA, Sinha Hikim AP, Clegg ED (1990) *Histological and Histopathological Evaluation of the Testis* (Cache River, Clearwater, FL).
16. Namekawa SH, et al. (2006) Postmeiotic sex chromatin in the male germline of mice. *Curr Biol* 16(7):660–667.
17. Zheng K, Wu X, Kaestner KH, Wang PJ (2009) The pluripotency factor LIN28 marks undifferentiated spermatogonia in mouse. *BMC Dev Biol* 9:38.
18. Buaas FW, et al. (2004) Plzf is required in adult male germ cells for stem cell self-renewal. *Nat Genet* 36(6):647–652.
19. Costoya JA, et al. (2004) Essential role of Plzf in maintenance of spermatogonial stem cells. *Nat Genet* 36(6):653–659.
20. Nakagawa T, Sharma M, Nabeshima Y, Braun RE, Yoshida S (2010) Functional hierarchy and reversibility within the murine spermatogenic stem cell compartment. *Science* 328(5974):62–67.

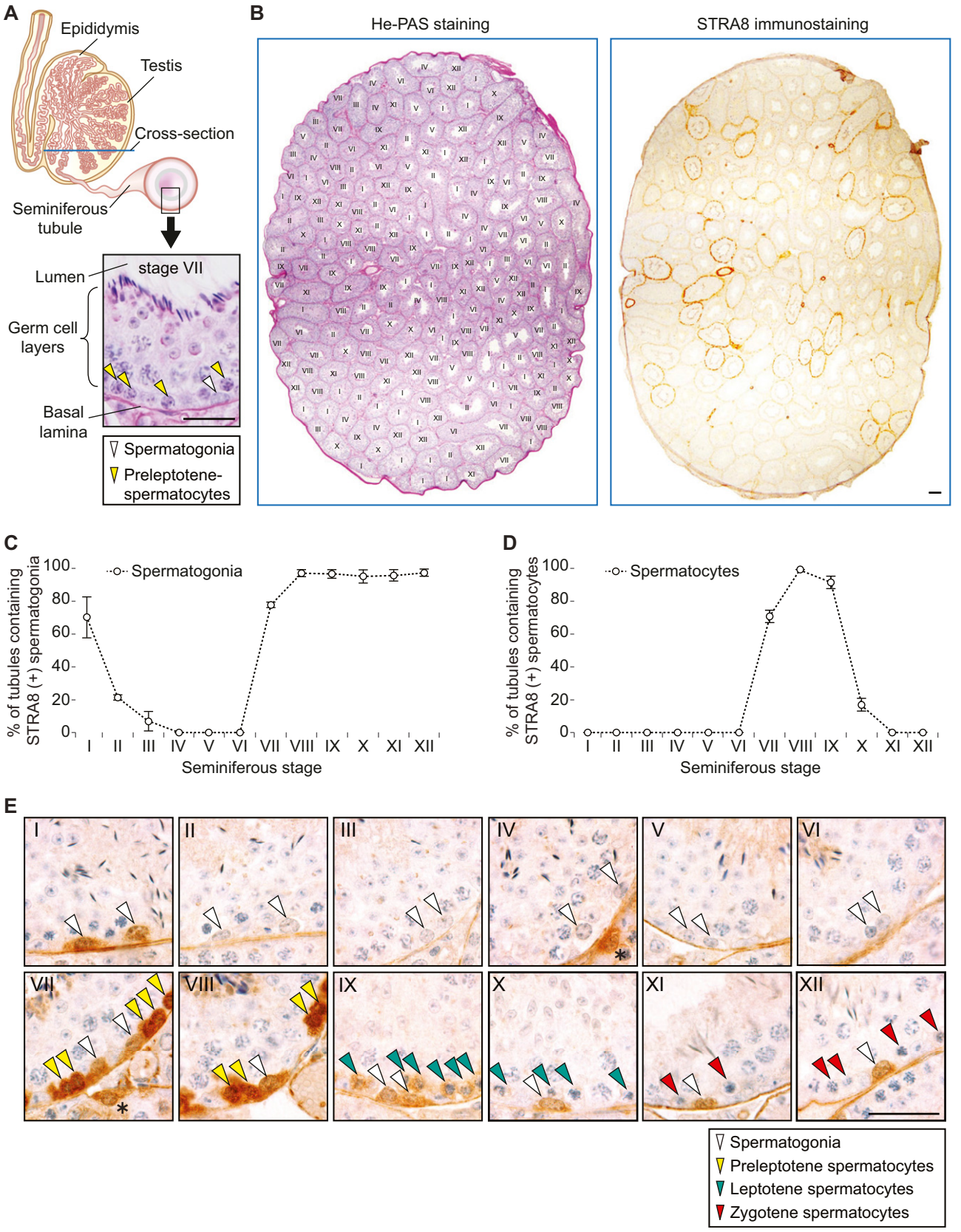

Fig. S1. STRA8 is cyclically expressed in both spermatogonia and spermatocytes. (*A*) Structure of the mouse testis comprising seminiferous tubules. In any given tubule cross-section, one observes germ cells at different steps in their development into spermatozoa. These germ-cell types are concentrically layered; undifferentiated spermatogonia lie on the basal lamina of the tubule, and germ cells move toward the tubule lumen as they differentiate (1). Germ-cell

Legend continued on following page

differentiation is precisely timed; hence, particular steps of development are always found together at the same time and place (Fig. 1*B*). Blue line indicates the orientation of testis cross-sections in *B*. Panel: A representative tubule cross-section in stage VII, stained with hematoxylin and periodic acid-Schiff (He-PAS). Arrowheads: spermatogonia (white) and preleptotene spermatocytes (yellow). (Scale bar, 30 μm.) (*B*) A scheme to determine the expression pattern of STRA8 in each testis tubule. One testis cross-section was immunostained for STRA8 (*Right*). The adjacent section was stained with He-PAS and used for staging (*Left*). (Scale bar, 100 μm.) (*C* and *D*) Percentage of tubules containing STRA8-positive spermatogonia (*C*) or STRA8-positive spermatocytes (*D*). All data are from wild-type, unperturbed mice. Error bars, mean ± SD. (*E*) Immunostaining for STRA8 on testis cross-sections. Roman numerals indicate stages. Arrowheads: spermatogonia (white), and preleptotene (yellow), leptotene (green), and zygotene spermatocytes (red). Asterisks indicate adjacent tubules containing STRA8 positive spermatogonia. (Scale bar, 30 μm.)

1. Oakberg EF (1956) A description of spermiogenesis in the mouse and its use in analysis of the cycle of the seminiferous epithelium and germ cell renewal. *Am J Anat* 99(3):391–413.

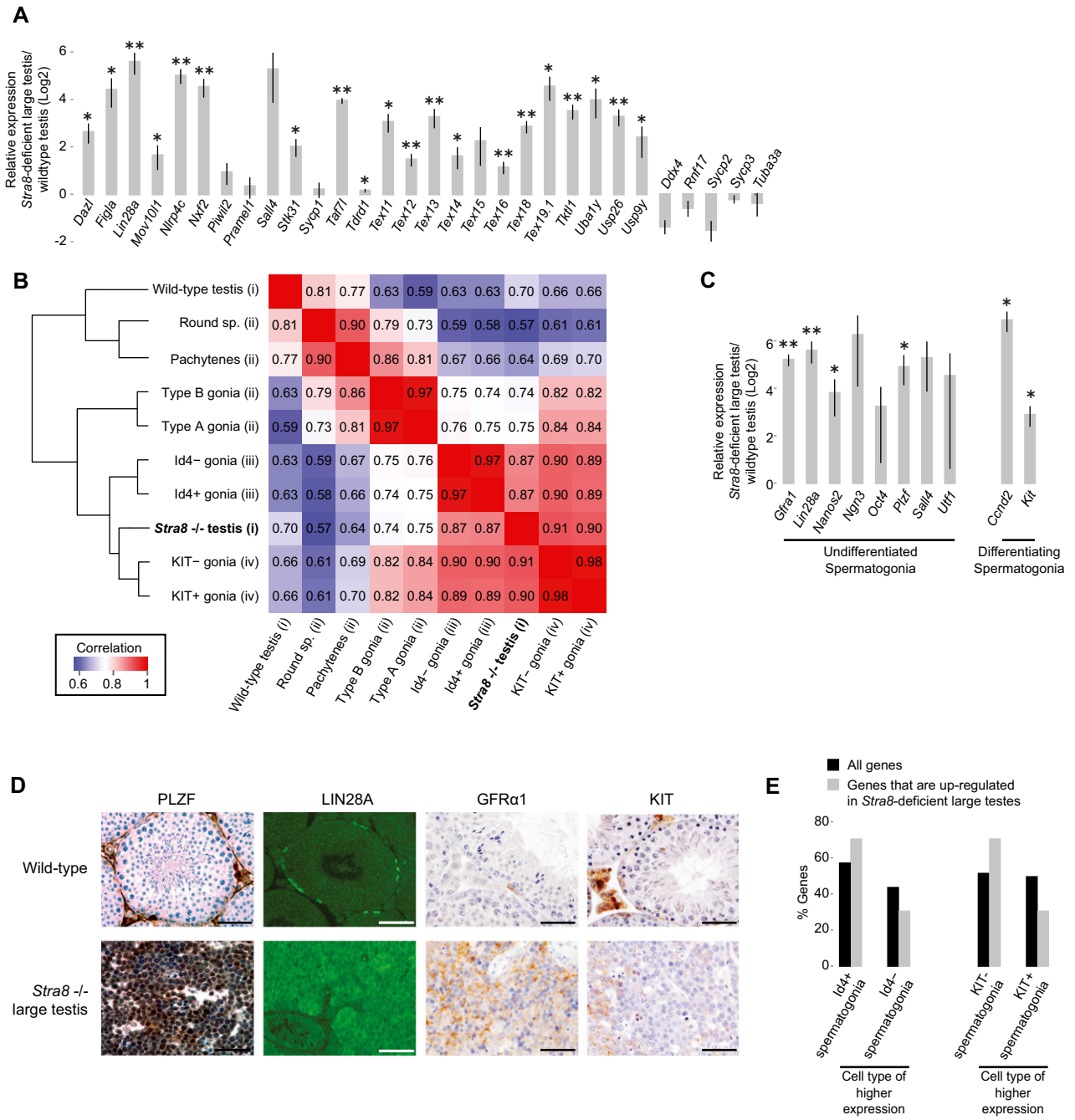

Fig. S2. Gene expression patterns of *Stra8*-deficient large testes resemble type A undifferentiated spermatogonia. (*A*) Expression of 30 spermatogonial marker genes (1) in *Stra8*-deficient large testes relative to adult wild-type testes. We show $\log_2$ ratios of normalized transcript counts (from mRNA-Seq). Error bars, mean ± SD $*P < 0.05$, $**P < 0.01$ (one-tailed Welch's *t* test). (*B*) Heat map of correlations between (*i*) our *Stra8*-deficient and wild-type testis RNA-seq data, and three other publically available genome-wide datasets: (*ii*) microarray data from type A spermatogonia, type B spermatogonia, pachytene spermatocytes, and round spermatids; (*iii*) mRNA-Seq data from Id4-GFP–positive and Id4-GFP–negative spermatogonia (1) (SRA accession no. SRP042067); and (*iv*) mRNA-Seq data from KIT-positive and KIT-negative spermatogonia (SRA accession no. DRP002386). Numbers are pairwise Spearman correlations between FPKMs/microarray expression values. Dendrogram represents complete linkage clustering of samples based on their correlations. (*C*) Expression of undifferentiated and differentiating spermatogonial marker genes, in *Stra8*-deficient large testes relative to adult wild-type testes. Undifferentiated spermatogonia marker genes: *Gfra1*; *Lin28a*; *Oct4* (a.k.a. *Pou5f1*); *Nanos2* (2, 3); *Ngn3* (4); *Plzf* (a.k.a. *Zbtb16*); *Sall4*; and *Utf1* (5, 6). Differentiating spermatogonia marker genes: *Ccnd2*, which is expressed exclusively in very early differentiating spermatogonia (7), and *Kit*, which is expressed in all differentiating spermatogonia. We show $\log_2$ ratios of normalized transcript counts (from mRNA-Seq). Error bars, mean ± SD $*P < 0.01$ (one-tailed Welch's *t* test). (*D*) Testis cross-sections from 1-y-old mice: wild-type (*Top*) and *Stra8*-deficient large (*Bottom*) testes. From left to right: immunostaining for PLZF, LIN28A, GFRα1, and KIT. (Scale bars, 50 μm.) (*E*) Percentage of genes whose expression is higher in (*Left*) Id4-GFP–positive spermatogonia or Id4-GFP–negative spermatogonia and (*Right*) KIT-positive spermatogonia or KIT-negative spermatogonia. Black bars (control), all analyzable genes (18,936 genes). Gray bars, 100 genes most significantly up-regulated in *Stra8*-deficient large testes relative to wild-type testes (Table S1).

1. Chan F, et al. (2014) Functional and molecular features of the Id4+ germline stem cell population in mouse testes. *Genes Dev* 28(12):1351–1362.
2. Sada A, Suzuki A, Suzuki H, Saga Y (2009) The RNA-binding protein NANOS2 is required to maintain murine spermatogonial stem cells. *Science* 325(5946):1394–1398.

3. Suzuki H, Sada A, Yoshida S, Saga Y (2009) The heterogeneity of spermatogonia is revealed by their topology and expression of marker proteins including the germ cell-specific proteins Nanos2 and Nanos3. *Dev Biol* 336(2):222–231.
4. Yoshida S, et al. (2004) Neurogenin3 delineates the earliest stages of spermatogenesis in the mouse testis. *Dev Biol* 269(2):447–458.
5. Guan K, et al. (2006) Pluripotency of spermatogonial stem cells from adult mouse testis. *Nature* 440(7088):1199–1203.
6. van Bragt MPA, et al. (2008) Expression of the pluripotency marker UTF1 is restricted to a subpopulation of early A spermatogonia in rat testis. *Reproduction* 136(1):33–40.
7. Beumer TL, Roepers-Gajadien HL, Gademan IS, Kal HB, de Rooij DG (2000) Involvement of the D-type cyclins in germ cell proliferation and differentiation in the mouse. *Biol Reprod* 63(6):1893–1898.

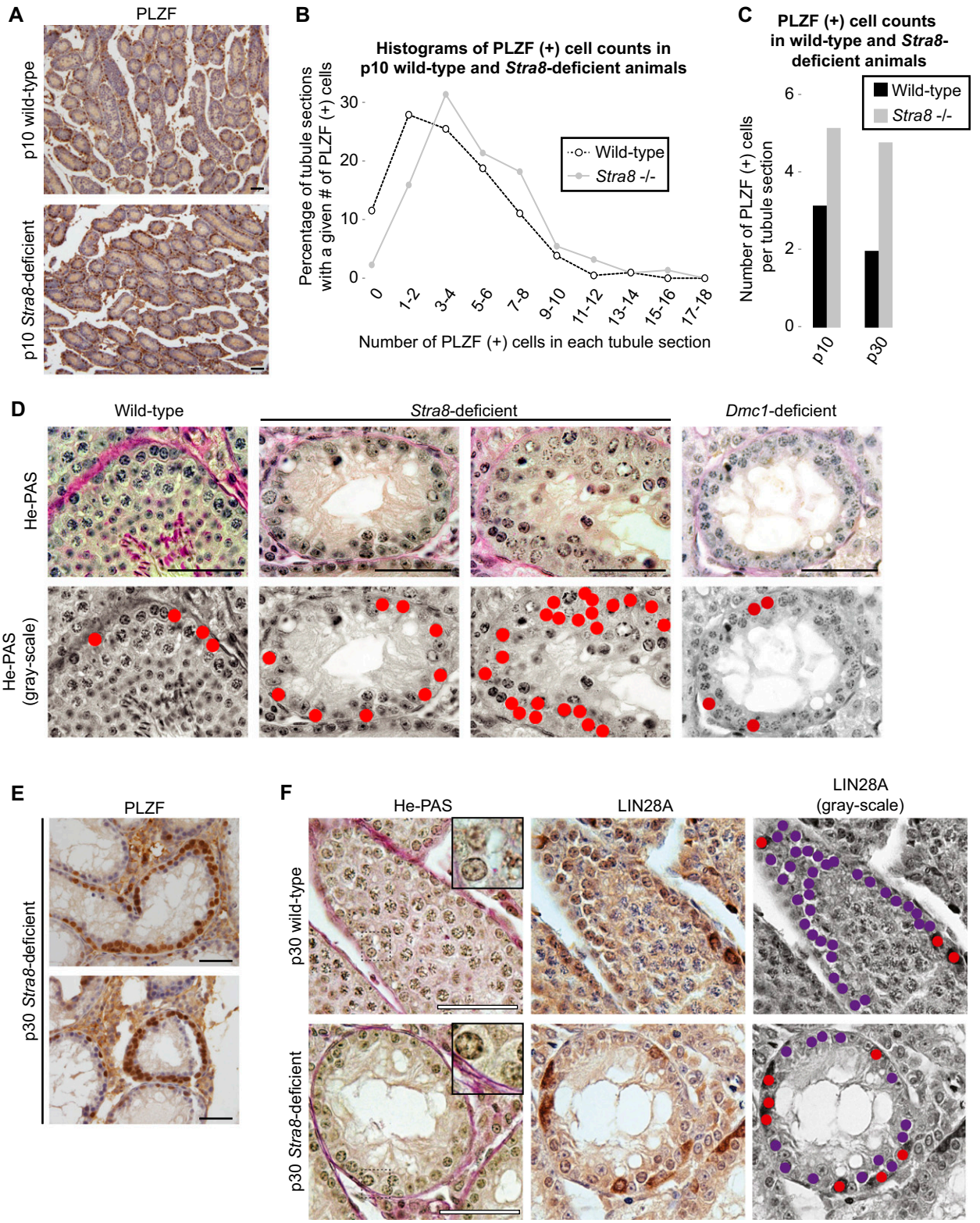

Fig. S3. LIN28A-positive and PLZF-positive spermatogonia accumulate at p10 and p30 in *Stra8*-deficient males. (*A*) Immunostaining for PLZF on postnatal day 10 (p10) testis sections: wild-type (*Top*) and *Stra8*-deficient (*Bottom*). (Scale bars, 50 μm.) (*B*) Histogram of number of PLZF-positive cells per tubule cross-section, in p10 wild-type and *Stra8*-deficient testes. Testes from one wild-type mouse and two *Stra8*-deficient mice were counted and averaged. (*C*) Number of PLZF-positive spermatogonia per tubule cross-section, in p10 and p30 wild-type and *Stra8*-deficient testes. One animal was counted for each condition (except for p10 *Stra8*-deficient, for which two animals were counted). (*D*) Testis cross-sections from p30 mice: wild-type (*Left*), *Stra8*-deficient (*Middle*), and *Dmc1*-deficient (*Right*). (*Top*) Sections stained with He-PAS. (*Bottom*) Grayscale versions of top panel, with red dots indicating type A spermatogonia. Spermatogonial clusters (close packing of type A spermatogonia in multiple layers) were observed in some *Stra8*-deficient tubules, but never in wild-type or *Dmc1*-deficient tubules. Because tubule size is reduced in both *Stra8*-deficient and *Dmc1*-deficient testes (owing to meiotic arrest), we conclude that the spermatogonial clusters are not

Legend continued on following page

simply a result of reduced tubule size. (Scale bars, 50 μm.) (*E*) Immunostaining for PLZF on p30 *Stra8*-deficient testis sections, showing clusters of PLZF-positive undifferentiated spermatogonia. (Scale bars, 50 μm.) (*F*) Testis cross-sections from p30 mice: wild-type (*Top*) and *Stra8*-deficient (*Bottom*). These are representative of the tubule cross-sections used for counts of type B and LIN28A-positive spermatogonia (Fig. 3*D*). (*Left*) He-PAS stained section. Inset enlarges the boxed region. (*Middle*) Adjacent section, immunostained for LIN28A. (*Right*) Grayscale version of middle panel, with red dots indicating LIN28A-positive spermatogonia, and purple dots indicating type B spermatogonia. (Scale bars, 50 μm.)

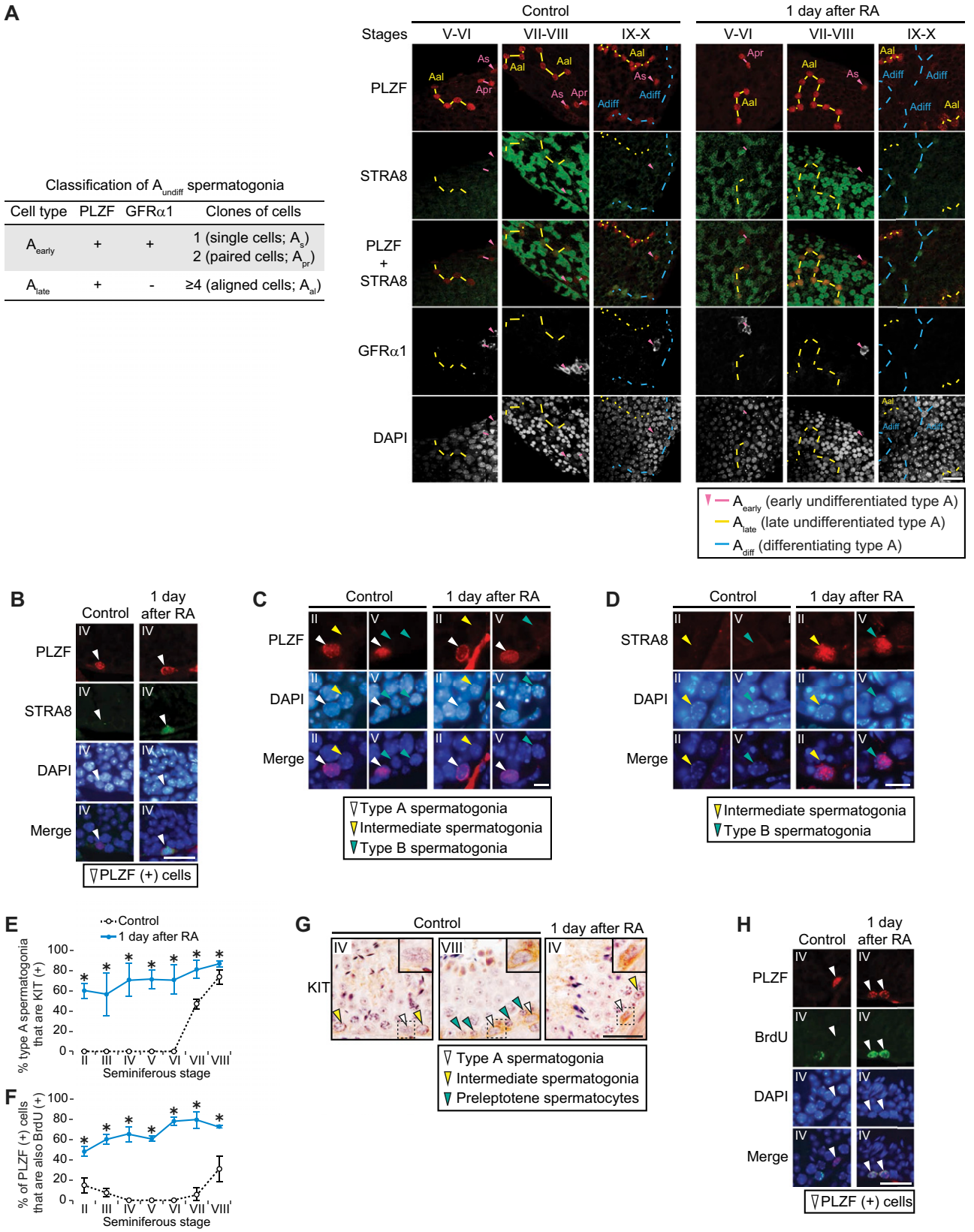

Fig. S4. Injected RA induces precocious STRA8 expression, KIT expression, and S phase entry. (*A*) Whole-mount immunostaining of the intact wild-type testis tubules shown in Fig. 4*A*, for PLZF (red), STRA8 (green), and GRFα1 (gray), with DAPI counterstain (gray). (PLZF and STRA8 panels are duplicated from Fig. 4*A*.) Dashed lines: putative interconnected chains of spermatogonia. Magenta labels: early undifferentiated type A spermatogonia (A_{early}). Yellow labels: late undifferentiated type A spermatogonia (A_{late}). A_s, A_{pr}, and A_{al}: A_{single} (isolated; arrowheads), A_{paired} (chains of 2), and $A_{aligned}$ (chains of ≥4) spermatogonia.

Legend continued on following page

Blue labels: differentiating type A spermatogonia (A_{diff}). A_{early} identified as PLZF-positive, GRFα1-positive A_s and A_{pr}; A_{late} identified as PLZF-positive, GFRα1-negative A_{al}. (Scale bar, 30 μm.) (*B*) Immunostaining for PLZF (red) and STRA8 (green), with DAPI counterstain (blue), on control and RA-injected testis cross-sections in stage IV. Arrowheads: PLZF-positive cells. (Scale bar, 30 μm.) (*C*) PLZF is expressed only in type A spermatogonia, not in intermediate or type B spermatogonia, in controls and 1 d after RA injection. Immunostaining for PLZF (red), with DAPI counterstain (blue), on control and RA-injected testis cross-sections in stages II and V. Arrowheads: type A (white), intermediate (yellow), and type B (green) spermatogonia. (Scale bar, 10 μm.) (*D*) Immunostaining for STRA8 (red), with DAPI counterstain (blue), on control and RA-injected testis cross-sections in stages II and V. Arrowheads: premeiotic germ cells, specifically intermediate (yellow) and type B (green) spermatogonia. (Scale bar, 10 μm.) (*E*) Percentage of type A spermatogonia that are positive for KIT in testis cross-sections, in controls or 1 d after RA injection. Error bars, mean ± SD $*P < 0.01$(one-tailed Welch's *t* test). (*F*) Percentage of PLZF-positive cells that are also positive for BrdU in testis cross-sections, in controls or 1 d after RA injection. Error bars, mean ± SD $*P < 0.01$(one-tailed Welch's *t* test). (*G*) Immunostaining for KIT, on control and RA-injected testis cross-sections in stages IV and VIII. Insets enlarge boxed regions. Arrowheads: type A (white) and intermediate (yellow) spermatogonia, and preleptotene spermatocytes (green). (Scale bar, 30 μm.) (*H*) Immunostaining for PLZF (red) and BrdU (green), with DAPI counterstain (blue), on control and RA-injected testis cross-sections in stage IV. Arrowheads: PLZF-positive cells. (Scale bar, 30 μm.)

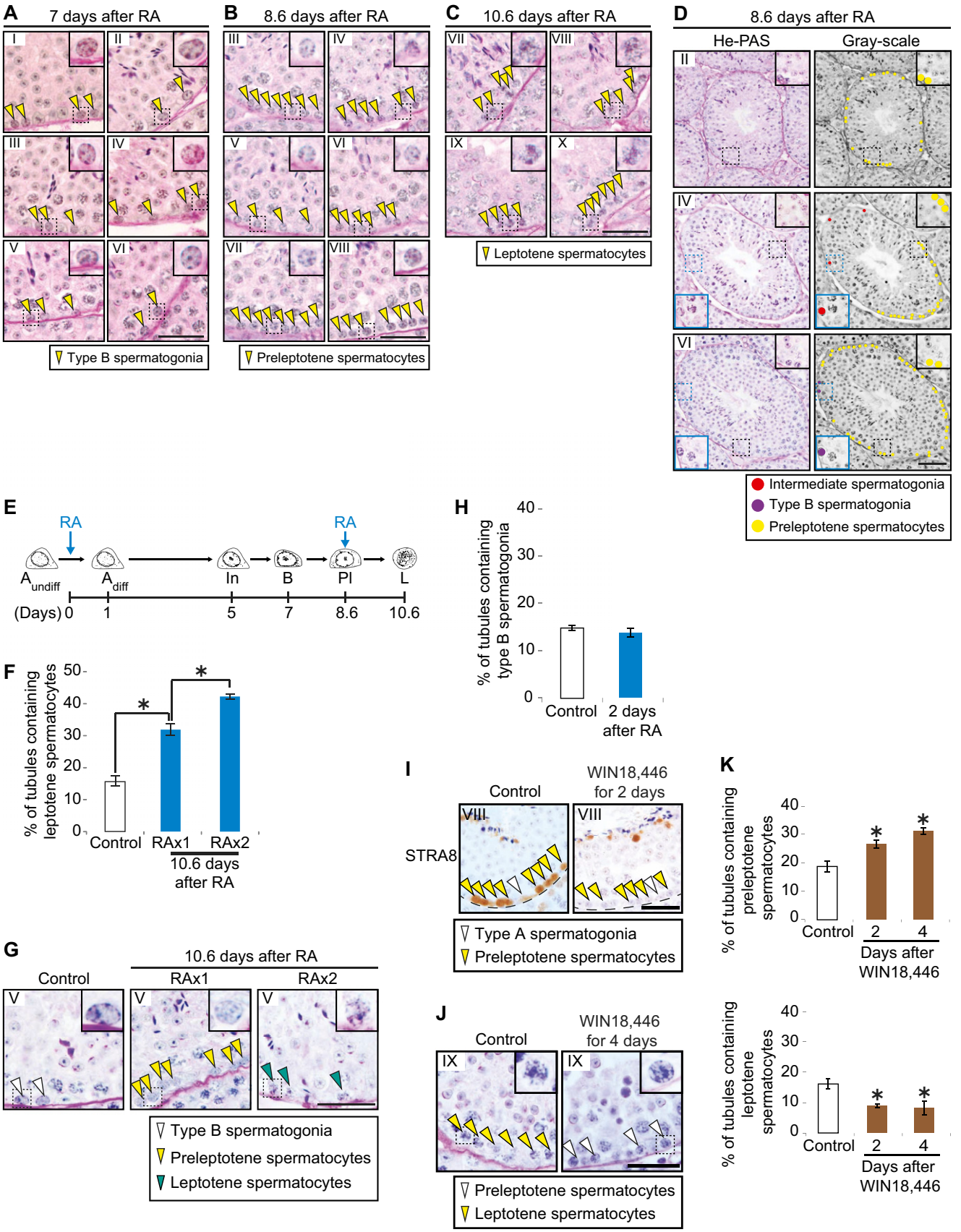

Fig. S5. Injected RA induces premature spermatogonial differentiation in stages II–VI and premature meiotic initiation in stage VI. (*A–C*) RA-injected testis cross-sections, stained with He-PAS. Roman numerals indicate stages. Arrowheads in *A*: type B spermatogonia. Arrowheads in *B*: preleptotene spermatocytes.

Legend continued on following page

Arrowheads in *C*: leptotene spermatocytes. Insets enlarge boxed regions. (Scale bars, 30 μm.) (*D*) The entire tubule images of RA-injected testis cross-sections in stages II, IV, and VI, stained with He-PAS. Insets (blue and black) enlarge boxed regions. (*Left*) He-PAS stained section. (*Right*) Grayscale version of left panel. Red, purple, and yellow dots indicate Intermediate spermatogonia, type B spermatogonia, and preleptotene spermatocytes, respectively. At 8.6 d after RA injection, the tubules in stages II–VI contained predominantly preleptotene spermatocytes, with only a few Intermediate and type B spermatogonia. This result indicates that, at the time of RA injection, most (although not all) undifferentiated spermatogonia in stages II–VI successfully underwent precocious spermatogonial differentiation. (Scale bars, 50 μm.) (*E*–*G*) Two RA injections induced meiotic initiation in all preleptotene spermatocytes present in stages II–VIII. At 10.6 d after a single RA injection, leptotene spermatocytes were present only in stages VI–X (Fig. 5 *F* and *G*). (If all preleptotene spermatocytes in stages II–VIII had initiated meiosis, we would expect to observe leptotene spermatocytes throughout stages V–X. See Table S2 for details.) Because RA is required for meiotic initiation, we reasoned that a second injection of RA might be required to induce meiotic initiation in all preleptotene spermatocytes present in stages II–VIII. Thus, we gave a second injection of RA, 8.6 d after the first injection, and collected testes after 10.6 d (*E*). We observed leptotene spermatocytes in stages V–X (*F* and *G*). (*E*) Diagram of germ-cell development after two injections of RA (8.6 d apart). Testes were harvested 10.6 d after the first RA injection. A_{undiff}, A_{diff}, In and B: undifferentiated type A, differentiating type A, intermediate, and type B spermatogonia. Pl and L: preleptotene and leptotene spermatocytes. (*F*) Percentage of tubules containing leptotene spermatocytes, in control or RA-injected testis cross sections. Mice were injected with RA once (RAx1) or twice (RAx2). Error bars, mean ± SD $*P < 0.01$ (Tukey–Kramer test). (*G*) Control and RA-injected testis cross-sections in stage V, stained with He-PAS. Mice were injected with RA once (RAx1) or twice (RAx2). Arrowheads: intermediat e spermatogonia (white) and leptotene spermatocytes (yellow). Insets enlarge boxed regions. (Scale bars, 30 μm.) (*H*) Percentage of tubules containing type B spermatogonia, in control or RA-injected testis cross-sections. Error bars, mean ± SD. (*I*) Immunostaining for STRA8 on testis cross-sections in stage VIII. Sections are from control mice, and from mice treated with WIN18,446 for 2 d. Dashed lines, basal laminae. Arrowheads: type A spermatogonia (white) and preleptotene spermatocytes (yellow). (Scale bar, 30 μm.) (*J*) Testis cross-sections in stage IX, stained with He-PAS. Sections are from control mice and from mice treated with WIN18,446 for 4 d. Arrowheads: preleptotene spermatocytes (white) and leptotene spermatocytes (yellow). Insets enlarge boxed regions. (Scale bar, 30 μm.) (*K*) Percentage of tubules containing preleptotene spermatocytes (*Top*) or leptotene spermatocytes (*Bottom*), in testis cross-sections from control or WIN18,446-treated mice. Error bars, mean ± SD $*P < 0.01$, compared with control (Dunnett's test). See also Table S2.

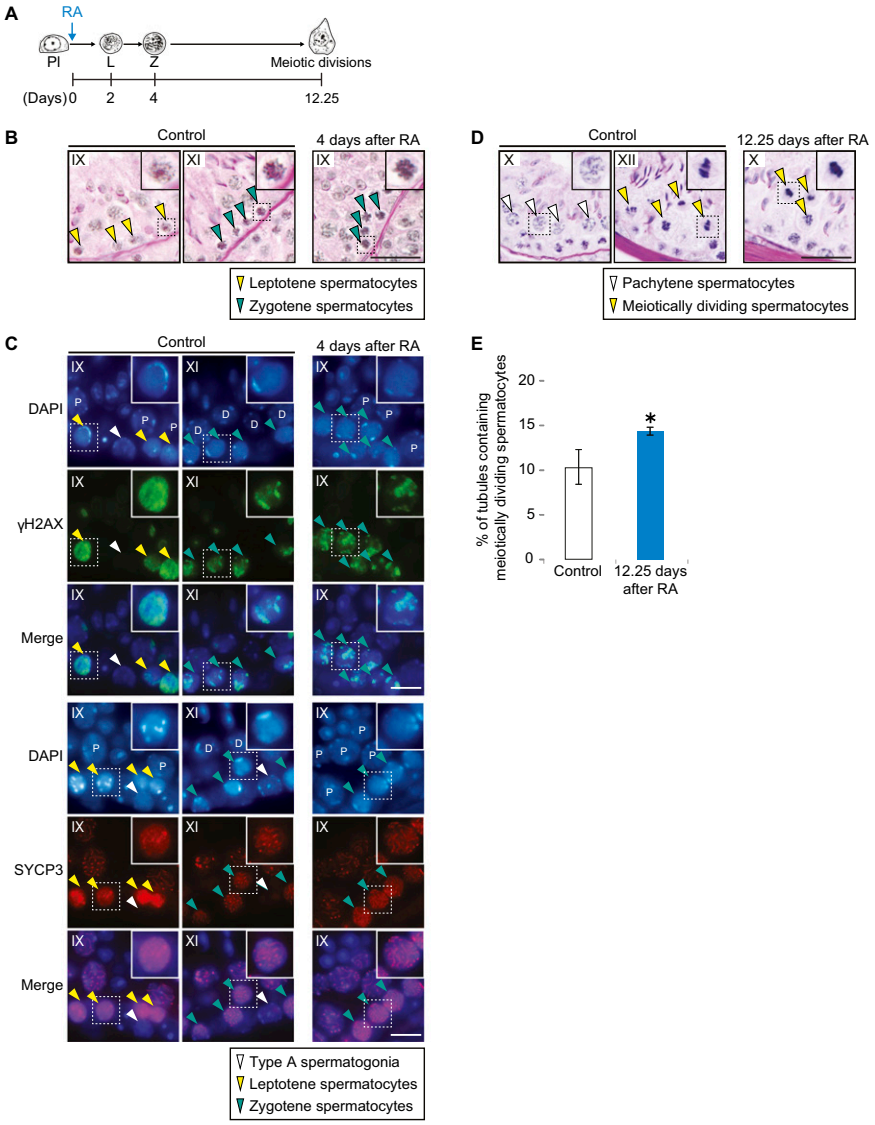

Fig. S6. After RA injection, precocious leptotene spermatocytes undergo meiotic progression and meiotic divisions. (*A*) Diagram of spermatocyte development after RA injection. L, Pl, and Z: leptotene, preleptotene, and zygotene spermatocytes. (*B*) Control and RA-injected testis cross-sections, stained with He-PAS. Roman numerals indicate stages. Arrowheads: leptotene (yellow) and zygotene (green) spermatocytes. Insets enlarge boxed regions. (Scale bar, 30 μm.) (*C*) Immunostaining for γH2AX (green) and SYCP3 (red), with DAPI counterstain, on control and RA-injected testis cross-sections. Roman numerals indicate stages. Arrowheads: type A spermatogonia (white), and preleptotene (yellow) and leptotene (green) spermatocytes. D and P: diplotene and pachytene spermatocytes. Insets enlarge boxed regions. (Scale bars, 10 μm.) (*D*) Control and RA-injected testis cross-sections, stained with He-PAS. Roman numerals indicate stages. Arrowheads: pachytene (white) and meiotically dividing (yellow) spermatocytes. Insets enlarge boxed regions. (Scale bar, 30 μm.) (*E*) Percentage of tubules containing meiotically dividing spermatocytes, in control or RA-injected testis cross-sections. Error bars, mean ± SD $*P < 0.01$ (one-tailed Welch's *t* test).

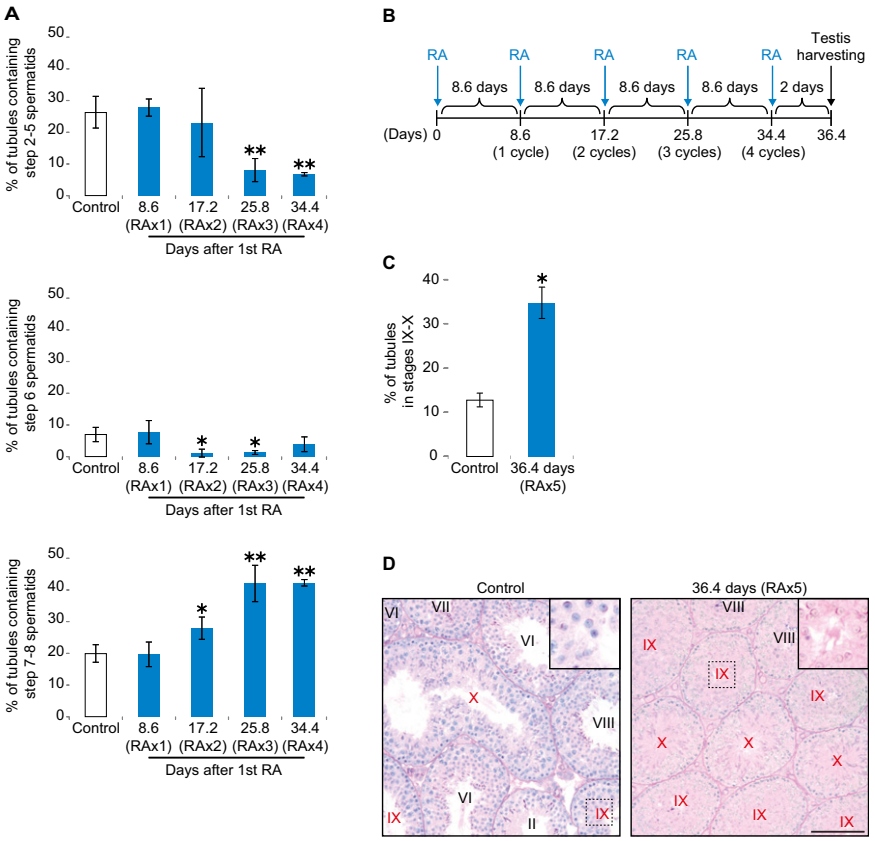

Fig. S7. Successive RA injections confirm distinct competencies for spermatogonial differentiation and meiotic initiation. (*A*) Percentage of tubules containing spermatids at various steps of postmeiotic differentiation, steps 2–5 (*Top*), step 6 (*Middle*), or steps 7–8 (*Bottom*), in control or RA-injected testis cross-sections. Error bars, mean ± SD $*P < 0.05$, $**P < 0.01$, compared with control (Dunnett's test). (*B–D*) Successive RA injections can drive release of spermatozoa. (*B*) Diagram of five successive RA injections. Testes were harvested 36.4 d after the first RA injection. (*C*) Percentage of tubules in stages IX–X of the seminiferous cycle, in controls and after five RA injections. Tubules in stages IX–X have recently undergone release of spermatozoa. Error bars, mean ± SD $*P < 0.01$ (two-tailed Welch's *t* test). (*D*) Testis cross-sections, stained with He-PAS, in controls (*Left*) or after five RA injections (*Right*). The cross-section areas with the highest frequency of stage IX–X tubules (red) were selected. Roman numerals indicate stages. Insets enlarge boxed regions. (Scale bar, 100 μm.)

Table S1. One hundred genes most significantly up-regulated in *Stra8*-deficient large (large) testes, relative to wild-type (WT) testes

No.	Gene name	Log_2(fold-change) (large/WT)	*P* value (false discovery rate-corrected)
1	*Ccnd2*	6.68	4.86E-59
2	*Phlda2*	9.44	2.06E-58
3	*Gpnmb*	8.76	4.26E-54
4	*Dkk3*	7.22	5.23E-54
5	*Upp1*	6.76	2.98E-52
6	*Irf1*	5.95	9.11E-51
7	*Fbxo41*	6.36	3.18E-50
8	*Dapk2*	6.44	2.03E-49
9	*Slc38a4*	6.97	3.82E-48
10	*Spp1*	7.86	6.36E-48
11	*Piwil4*	7.29	7.03E-48
12	*Rrad*	7.23	8.72E-48
13	*Afp*	7.48	2.54E-47
14	*Cd9*	6.45	5.71E-47
15	*Pramef12*	5.79	2.68E-46
16	*Mobp*	6.78	7.48E-45
17	*Glipr2*	6.30	1.22E-44
18	*Mmp2*	6.16	3.24E-44
19	*Pgc*	9.79	4.08E-44
20	*Abcc8*	6.00	6.17E-44
21	*Nphs1*	9.37	1.60E-43
22	*Asphd2*	6.70	4.77E-43
23	*Gnb4*	5.71	9.92E-43
24	*Tmem40*	7.94	2.12E-42
25	*A230065- H16Rik*	6.45	4.88E-42
26	*Pnma5*	5.44	5.13E-42
27	*Lin28a*	5.33	7.08E-42
28	*Foxf1a*	6.99	1.15E-41
29	*Lamb1*	4.91	1.67E-41
30	*Cpm*	6.04	3.76E-41
31	*Bmpr1b*	6.84	3.09E-40
32	*Gfra1*	5.00	4.34E-40
33	*Dctd*	5.16	4.91E-40
34	*Serpine2*	5.44	1.62E-39
35	*Depdc7*	5.78	2.62E-39
36	*Clec7a*	7.32	7.26E-39
37	*Hoxb4*	7.37	8.89E-39
38	*Erg*	5.63	1.01E-38
39	*Tph1*	8.92	1.58E-38
40	*Apba2*	6.45	3.08E-38
41	*Tro*	5.04	3.11E-38
42	*Nfkbid*	6.91	3.60E-38
43	*Cacnb3*	5.40	3.93E-38
44	*Slc15a3*	6.44	4.94E-38
45	*9130401-M01Rik*	5.02	5.07E-38
46	*Slc26a5*	8.28	2.59E-37
47	*Mmp12*	35.00	2.72E-37
48	*Alkbh2*	6.29	2.77E-37
49	*Six4*	4.91	4.42E-37
50	*Fbxo32*	5.23	9.93E-37
51	*Atp6v0d2*	8.26	2.82E-36
52	*Cenpa*	4.91	3.71E-36
53	*Igfbpl1*	7.45	5.52E-36
54	*Ldlrad3*	5.07	5.61E-36
55	*Nefm*	7.51	6.17E-36
56	*Pde9a*	5.18	1.78E-35
57	*Crabp1*	4.78	2.49E-35
58	*Coro1a*	6.01	5.02E-35
59	*Hoxa1*	6.43	1.19E-34
60	*Klf11*	4.42	6.64E-34
61	*Hrh1*	5.14	7.75E-34
62	*Dctpp1*	4.88	9.38E-34

Table S1. Cont.

No.	Gene name	Log_2(fold-change) (large/WT)	*P* value (false discovery rate-corrected)
63	*Onecut2*	5.37	1.21E-33
64	*Ret*	5.09	1.59E-33
65	*Dlk1*	4.90	2.11E-33
66	*Sntg2*	5.95	2.40E-33
67	*Nptx1*	5.61	2.81E-33
68	*Gng13*	6.10	3.74E-33
69	*Morc1*	4.58	3.80E-33
70	*Ankrd26*	4.80	4.14E-33
71	*Ly6g6e*	6.97	4.89E-33
72	*Trpv4*	5.08	6.34E-33
73	*Gprc5c*	6.47	6.94E-33
74	*Dlk2*	5.72	8.87E-33
75	*Nlrp4c*	4.80	1.36E-32
76	*Grik3*	4.83	1.57E-32
77	*2610524-H06Rik*	5.52	1.84E-32
78	*Prtg*	4.95	2.12E-32
79	*Zrsr2*	4.27	2.96E-32
80	*Sertad4*	4.30	3.11E-32
81	*4933427-D06Rik*	4.51	3.19E-32
82	*Tpbg*	5.52	3.62E-32
83	*Zbtb16*	4.66	3.63E-32
84	*Slc4a5*	4.75	3.81E-32
85	*Hyal2*	4.29	4.69E-32
86	*Dgki*	5.25	5.50E-32
87	*Slc30a10*	33.80	6.55E-32
88	*Mdh2*	4.33	1.04E-31
89	*Gcat*	4.49	1.15E-31
90	*Nthl1*	4.83	1.42E-31
91	*Osbpl3*	4.70	1.53E-31
92	*Dbndd2*	4.19	1.56E-31
93	*Fsd1*	4.43	2.09E-31
94	*Cnn3*	4.74	2.41E-31
95	*Oasl2*	5.05	2.44E-31
96	*Armcx4*	5.45	2.52E-31
97	*Lgals3*	5.54	2.68E-31
98	*Hoxb2*	6.09	2.77E-31
99	*Tex19.1*	4.33	2.93E-31
100	*Il13ra1*	4.68	3.45E-31

Table S2. Progression of germ cells through the seminiferous stages after RA-induced precocious spermatogonial differentiation

		Expected stage progression							Observed stage progression
Days after RA	Germ-cell type	Broken into individual stages						Full stage range	Full stage range
0	A_{diff} spermatogonia	II/III	IV	V	VI	VII	VIII	II–VIII	II–VIII
7	Type B spermatogonia	XII/I	I	II	II	IV	V/VI	XII–VI	XII–VI
8.6	Preleptotene spermatocytes	II/III	IV	V	VI	VII	VIII	II–VIII	II–VIII
10.6	Leptotene spermatocytes	V/VI	VI/VII	VII	VIII	IX	X/XI	V–X	VI–X (1 RA injection) V–X (2 RA injections)

Table S3. Antibodies and conditions for immunostaining

	Primary antibody					
Antigen	Type	Source (catalog no.)	Incubation condition	Blocking condition	Detection type	Secondary antibody
BrdU	Rat monoclonal	AXYLL (OBT0030)	1:500 o/n 4 °C	2.5% donkey serum	Fluorescence	FITC-conjugated 1:200, 60 min r.t.
DAZL	Mouse monoclonal	AbD Serotec (MCA2336)	1:100 30 min r.t.	5% BSA	Colorimetric	PowerVision Poly-HRP IgG reagent, 30 min r.t
GFRα1	Goat polyclonal	R&D systems (AF560)	1:100 o/n 4 °C	2.5% donkey serum	Fluorescence	Dylight 649-conjugated, 1:200, 45 min r.t.
γH2AX	Mouse monoclonal	Upstate Biotechnology (05-636)	1:100 o/n 4 °C	2.5% donkey serum	Fluorescence	FITC-conjugated 1:200, 45 min r.t.
KIT	Mouse monoclonal	Cell Signaling Technology (3074)	1:100 120 min r.t.	2.5% normal horse serum	Colorimetric	Anti-rabbit ImmPRESS peroxidase reagent 30 min r.t.
LIN28A	Rabbit polyclonal	Abcam (ab46020)	1:200 o/n 4 °C	5% BSA and 2.5% normal horse serum	Colorimetric	Anti-goat ImmPRESS peroxidase reagent 10 min r.t.
	Goat polyclonal	R&D Systems (AF3757)	1:100 o/n 4 °C	1% BSA and 5% donkey serum	Fluorescence	Biotinylated horse anti-goat 1:200, 60 min r.t.
PLZF	Mouse monoclonal	Calbiochem (2A9)	1:100 30 min r.t.	5% BSA	Colorimetric	PowerVision Poly-HRP IgG reagent, 30 min r.t
	Mouse monoclonal	Calbiochem (OP128)	1:100 o/n 4 °C	2.5% donkey serum	Fluorescence	DyLight 549-conjugated 1:200, 45 min r.t.
STRA8	Rabbit polyclonal	Abcam (Ab49405)	1:200 30 min r.t.	5% BSA or 2.5% normal horse serum	Colorimetric	Anti-rabbit ImmPRESS peroxidase reagent 30 min
	Rabbit polyclonal	Abcam (Ab49405)	1:500 o/n 4 °C	2.5% donkey serum	Fluorescence	DyLight 488- or Rhodamine Red X- conjugated 1:200, 45 min r.t.
SYCP3	Mouse monoclonal	Santa Cruz Biotechnology (sc-74569)	1:100 o/n 4 °C	2.5% donkey serum	Fluorescence	Rhodamine Red X-conjugated 1:200, 45 min r.t
	Rabbit polyclonal	Abcam (ab15092)	1:1,000 o/n 4 °C	2.5% donkey serum	Fluorescence	Rhodamine Red X-conjugated 1:200, 45 min r.t.

o/n, overnight; r.t, room temperature.